Research article

Journal of RAMAN SPECTROSCOPY

Received: 11 August 2015 Revised: 30 March 2016 Accepted: 7 April 2016 Published online in Wiley Online Library

(wileyonlinelibrary.com) DOI 10.1002/jrs.4946

Directionally enhanced probe for side-illumination Tip enhanced spectroscopy

Hongming Shen,[a] Guowei Lu,[a,b]* Zhengmin Cao,[a] Yingbo He,[a] Yuqing Cheng,[a] Jiafang Li,[c] Zhi-Yuan Li[c] and Qihuang Gong[a,b]

We investigate the high performance of an apertureless near-field probe consisting of a tapered metal tip with periodic shallow surface grooves. The spontaneous emission of a single emitter near the apex is systematically analyzed for side-illumination tip enhanced spectroscopy scheme. In contrast to a conventional bare tapered tip, the corrugated probe not only strongly enhances the local excitation field, but also modulates the emission directivity, leading to high collection efficiency and signal-to-noise ratio. Specifically, we propose that an asymmetric tip enhanced spectroscopy probe containing two different length nanorods at the apex realizes unidirectional emissions. The radiation pattern is sensitive to the emission wavelengths and the emitter positions, which can increase the signal-to-noise ratio through suppression of the undesired signal. The proposed asymmetrical corrugated probe possesses a wide range of potential applications, including increasing the detection efficiency of tip enhanced spectroscopy at the single molecule level. Copyright © 2016 John Wiley & Sons, Ltd.

Keywords: directional emission; plasmonics; apertureless probe; tip enhanced spectroscopy; spontaneous emission

Introduction

Nanoscale chemical analysis for heterogeneous surfaces or interfaces is becoming more and more important in multiple disciplines, including heterogeneous catalysis, molecular electronics, and biology.[1] Microscopic techniques that rely on the enhanced electric field near a sharp and laser irradiated metal tip, such as tip enhanced spectroscopy (TES), combine scanning probe microscopy (SPM) for high spatial resolution and optical spectroscopy for determining the chemical signatures of molecules. These are also known as 'apertureless' versions of scanning near-field optical microscopy.[2] The technique allows for the study of various spectroscopic signals, including one-photon or two-photon excited fluorescence,[3] coherent anti-Stokes Raman scattering,[4] spontaneous Raman scattering, harmonic generations, and time-resolved measurements.[5–7] Specifically, because the invention of tip-enhanced Raman scattering (TERS), TERS imaging experiments have been performed on single molecules, graphene, carbon nanotubes, and biological samples.[8–12]

With TERS gaining increasing importance and commercialization as a chemical analytical technique, questions about the rapidity of TERS imaging measurements arise. For example, to obtain an image with 256×256 pixels at an acquisition time at 0.5 s/pixel for weak Raman scatterers, a measurement will take approximately 9 h. Over this time, thermal drift of the SPM system can have a significant influence on the image quality, and possible photodegradation of the samples can also limit the total imaging time. Therefore, the collection time per pixel should be reduced as much as possible to avoid image distortion. Because of the inherently low Raman cross-section of most molecules, the excitation and detection of the scattered light must be efficient to allow for a short acquisition time.[13] Thus, highly efficient detectors, optical systems, and strongly enhanced metallic apertureless tips are required. Currently, optical detectors with single-photon detection capabilities are available, and current commercial optical systems present great efficiency. These factors have been optimized by some home-built systems, but they are still unlikely to significantly reduce the collection time of TERS imaging.

A metallic tip is the key device in TES as a local scatterer, which enhances and scatters the localized evanescent field towards the far-field. The near-field enhancement plays a central role in many nanoscale optical phenomena in plasmonics. The principle of TERS is related to surface-enhanced Raman scattering (SERS), where metallic nanoparticles or nanostructures lead to an enhancement by several orders of magnitude. For TERS, a metallic or metallized tip is illuminated by a focused laser beam and the resulting strongly enhanced electromagnetic field at the tip apex acts as a highly confined light source for Raman spectroscopic measurements. To date, a variety of optical probes have been proposed and applied to increase the spectroscopic response within a small sample volume.[14–17] Unfortunately, the excitation enhancement effect for a single tapered metal tip or gap antenna between the apex and metal substrate could be limited because of intrinsic nonradiative decay of the material. Most previous studies concentrated on the localized field enhancement effect because of localized surface plasmon (LSP) resonance or the lighting-rod effect.[18,19] Little research has focused on the directivity of signal

* *Correspondence to: Guowei Lu, Collaborative Innovation Center of Extreme Optics, Shanxi University, Taiyuan, Shanxi 030006, China. E-mail: guowei.lu@pku.edu.cn*

a *State Key Laboratory for Mesoscopic Physics & Collaborative Innovation Center of Quantum Matter, Department of Physics, Peking University, Beijing 100871, China*

b *Collaborative Innovation Center of Extreme Optics, Shanxi University, Taiyuan, Shanxi, 030006, China*

c *Laboratory of Optical Physics, Institute of Physics, Chinese Academy of Sciences, Beijing 100190, China*

emission modified by the metallic tips,[20] which would provide another way to improve the collection efficiency of the TES signal.

Recently, optical antennas have been utilized to manipulate the emission direction of single molecules, which may allow for a much shorter acquisition time.[21–23] In a previous study,[24] we reported on a 3-dimensional corrugated metal probe presenting beaming effect for the spontaneous emission from a single emitter, which improved the collection efficiency up to 25-fold compared with conventional bare tips. However, only the transmission-mode TES configuration was investigated and was limited to transparent samples. In this study, we extend our previous work with a theoretical exploration of the side-illumination TES scheme. Although side-illumination TERS with a metal substrate often provides highly efficient near-field enhancement, the low efficiency of the excitation and collection is an obvious weakness. Here, an asymmetric corrugated probe is proposed specifically for unidirectional and enhanced spontaneous emission, which improves both the excitation and collection efficiency. Numerical simulations show that this probe offers higher near-field enhancement factors and more effective directional control in comparison with a conventional bare tapered probe. This antenna design leads to a significant increase of the signal-to-noise ratio (SNR), which reduces the collection time of TERS imaging by an order of magnitude. The proposed probe thus provides a promising route in the development of directional enhanced emission related techniques.

Theoretical methods and models

Figure 1(a) illustrates the schematics of our proposed corrugated probe for TES. In the side-illumination scenario, a linear polarized beam is focused onto the tip/sample gap by a long working distance microscopic objective with an incidence angle of 60°. The strong local field at the apex effectively excites nearby single emitters or scatters. The enhanced spontaneous emission from a perpendicularly oriented emitter is collected using the same objective lens. In our simulations, the gold tip is modeled as a conical taper with an opening angle of 30° and tip-end radius of 10 nm. To improve the collection efficiency, the geometric parameters enabled more light to be directed towards the objective (Fig. 1b). These parameters were: groove period $G = 280$ nm, width $a = 140$ nm, depth $d = 40$ nm, groove number $N = 6$, and the tip-apex-to-first-groove distance $g = 280$ nm. To aid unidirectional emissions, we also placed two asymmetrical nanorods at the tip end as shown in Fig. 5(a); where one rod is longer than the other to avoid scanning the surface with two apexes. It should be noted that the fabrication of such asymmetric metal probes is very challenging in practical experiments. We thus propose a plausible way to fabricate the probe using nanofabrication methods. For example, the periodic gratings on the tip side surface can be made using a focused ion beam technique or 3D laser direct writing method.[18,25] For close-by dual asymmetric gold nanorods, a narrow slit can be cut at the tip apex using a focused ion beam, but the slit should deviate slightly from the tip central axis.

The finite-difference time-domain (FDTD) method is applied to simulate the emission process of a single dipole source near the metal tip.[26] This method has been widely used to calculate electromagnetic field distribution, scattering and absorption spectra, charge density distributions, and decay rates in the proximity of metallic nanostructures. We implemented a classical point current source placed under the tip end in the FDTD calculations. The dielectric permittivity of gold is taken from the Johnson and Christy data and fitted by the Drude–Lorentz dispersion model.[27] Perfectly matched layer (PML) techniques are used as the absorbing boundary conditions. We set the mesh size to 2 nm unless otherwise stated, so it should be noted that the simulations cannot be considered completely realistic. For most of these calculations, the tip-substrate distance is 20 nm. While a shorter tip-substrate distance (<5 nm) would be more ideal for the practical TERS experiment, the additional time and computer storage would be beyond the ability of our computation resources. We therefore investigated how the tip-substrate distance affects the angular far-field patterns (Fig. 3). The directional emission for a tip-substrate distance of 20 nm produced almost the same result as 4 nm tip-substrate distance, which suggests that the tip-substrate distance has little influence on the directivity, although the separation strongly affects the local field enhancement factor.

To obtain the far-field emission distribution, we first recorded the near-field data (**E** (t), **H** (t)) at two transformation surfaces S_L and S_R by applying FDTD simulations in the cylindrical coordinates (Fig. 1b). Because of the azimuthal symmetry, we can calculate the 3-dimensional directivity using the 2-dimensional simulation results. We then performed Fourier transform on these fields and calculated the surface electric ($\mathbf{J}_s$) and magnetic ($\mathbf{M}_s$) currents on the chosen surfaces S_L and S_R, respectively. According to the Near-Field to Far-Field (NTFF) transformation method,[28] we finally

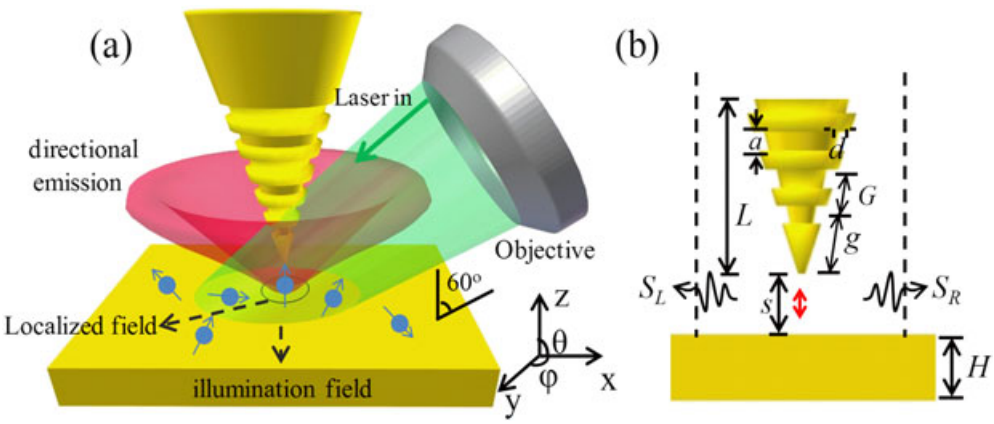

Figure 1. (a) Schematics of the proposed side-illumination/collection TERS configuration. A linear TM polarized beam passes through a long working distance objective with an incident angle of 60°. (b) Sketch of the metallic tip design: $G = g = 280$ nm, $a = 140$ nm, $d = 40$ nm, $N = 6$. The radius of curvature at the tip end is 10 nm with an opening angle of 30°.

Journal of RAMAN SPECTROSCOPY

derived angular directivity $D(\theta) = \pi P(\theta)/\int P(\theta)d\theta$ from the 2-dimensional simulation results,[29] where $P(\theta)$ is the angle-dependent time-averaged Poynting power density, and the integral is performed over the upper half space. To accurately utilize the simulation results, the transformation surfaces should be sufficiently large (S_L and S_R were approximately 9 μm long) and very close to the dipole source or metal tip to capture most of the fields that contribute to the far-field emission.

Results and discussion

The side-illumination TES presents several advantages to transmission-mode, such as a lack of limitation for transparent samples. However, since only a long working distance objective with low numerical aperture (NA) can be used in the side-illumination configuration, two issues need to be considered carefully: (i) the focal spot projected on the sample surface is usually very large (Fig. 1a), leading to strong optical background noise; (ii) the collection efficiency of the system is limited by the small detection angle because of the low NA objective lens. Consequently, the side-illumination TES approach always suffers from low SNR and collection efficiency.

Our aim was to improve the excitation and collection efficiency of the side-illumination TES, which is helpful for sensitive single molecule detection. We first considered the local field intensity in the excitation process based on 3D-FDTD simulations. In the simulations, the structured tip is under side-illumination by a *z*-polarized plane wave at a wavelength of 785 nm (Fig. 2a). It should be noted that the optimized response wavelength can be tuned by the corrugated probe parameters. The Yee cell size is set to 5 nm. Figures 2(b) and 2(c) show the dominant *z*-component electric field distribution $|E_z|^2/|E_{in}|^2$ in the *x*–*z* plane for a probe without and with gratings, respectively, where E_{in} is the incoming excitation field amplitude. For both of these cases, we observed a strong and highly localized field at the tip apex because of the lighting-rod effect of the sharp tip. With the corrugated tip, the maximum field enhancement *M* reaches up to 3755-fold, which is approximately 25 times higher than the bare tip (148-fold). The corrugated gratings provide the necessary momentum to match conditions for efficient surface plasmon polaritons (SPPs) coupling.[23] Figures 2(d) and 2(e) display the normalized curves of local field intensity along line *z* and in the *x* direction, respectively. The curve profiles of both are almost the same, indicating the gratings strongly enhance the field intensity, but do not affect its spatial distribution. This distribution is related to the spatial resolution (~18 nm) of the TES probe.[24]

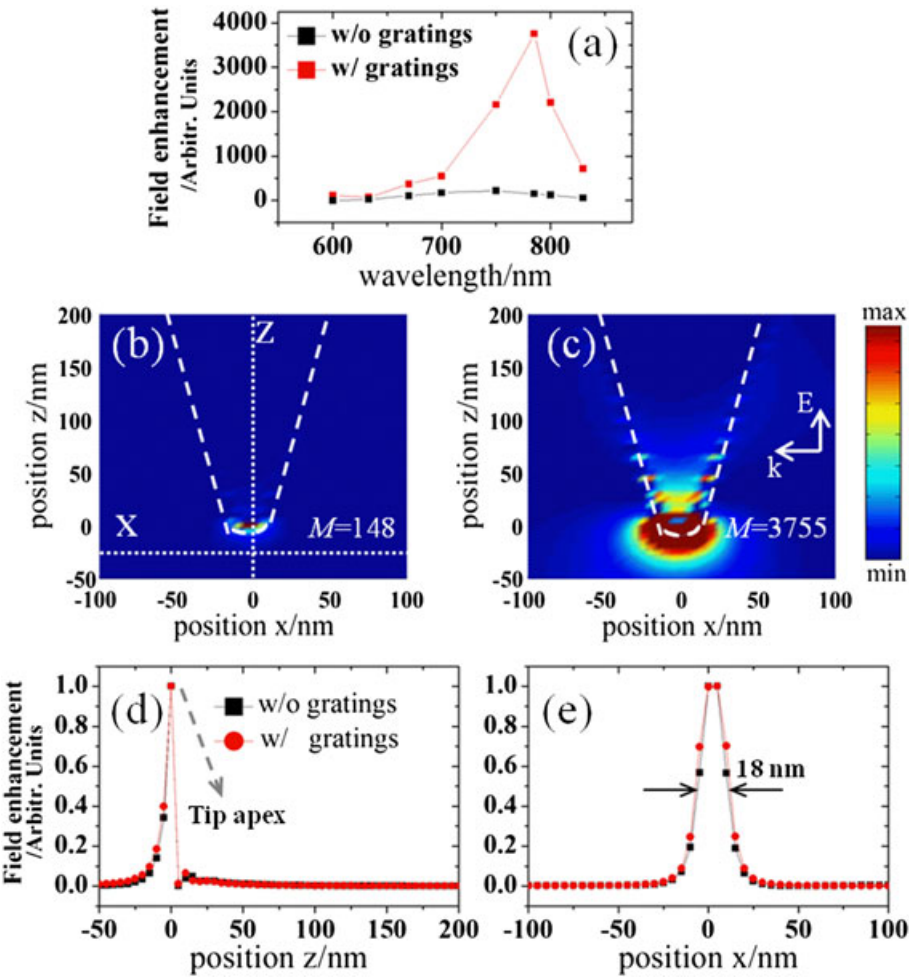

Figure 2. Localized excitation enhancements based on 3D-FDTD simulations. (a) Field enhancement $|E_z|^2/|E_{in}|^2$ as a function of wavelength. (b) and (c) demonstrate the electric field distribution for a tip without and with gratings in free space, respectively, while (d) and (e) show the normalized curves of local field enhancements along line profile *z* (along the tip axis) and in the *x* (at a surface 5 nm under the tip apex) direction. For the corrugated tip, the maximum field enhancement *M* at the tip apex is 3755-fold, 25 times higher than a bare tip.

Figure 3 demonstrates the calculated angular emission directivity obtained with the NTFF method. A *z*-oriented dipole emitter at 670 nm, corresponding to the emission band of the widely used Cyanine 5 dye molecule or fluorescent nanodiamond, is placed at a distance of 10 nm above the Au substrate. We compared three cases: (i) an isolated dipole emitter above the Au substrate; (ii) an emitter coupled to a tip without and (iii) with corrugated gratings. We assumed a 0.5 NA objective with maximum detectable angle of ±30°, fixed at an angle of 30°with respect to the tip axis. To quantify the collection efficiency of the system, we defined the factor $\kappa = P_1/P_2$, where $P_1 = \int_0^{\frac{\pi}{3}} P(\theta)d\theta$ is the power within the detectable angle of the objective and $P_2 = \int_0^{\pi} P(\theta)d\theta$ is the total power radiated to the upper half space for the 2-dimensional simulation

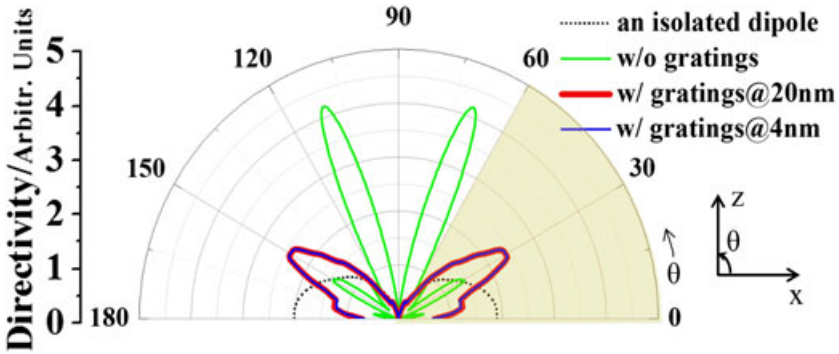

Figure 3. Calculated far-field radiation patterns in the *x*–*z* plane of a *z*-oriented dipole ($\lambda = 670$ nm) close to the metal substrate for three cases: an isolated dipole emitter (black dotted line), an emitter coupled to a tip without (green solid line) and with gratings (red solid line). The separation *s* between the tip and the gold substrate (thickness $H = 100$ nm) is 20 nm with a *z*-oriented dipole emitter placed in the middle. For comparison, we also calculated these patterns for a smaller tip-substrate distance of 4 nm.

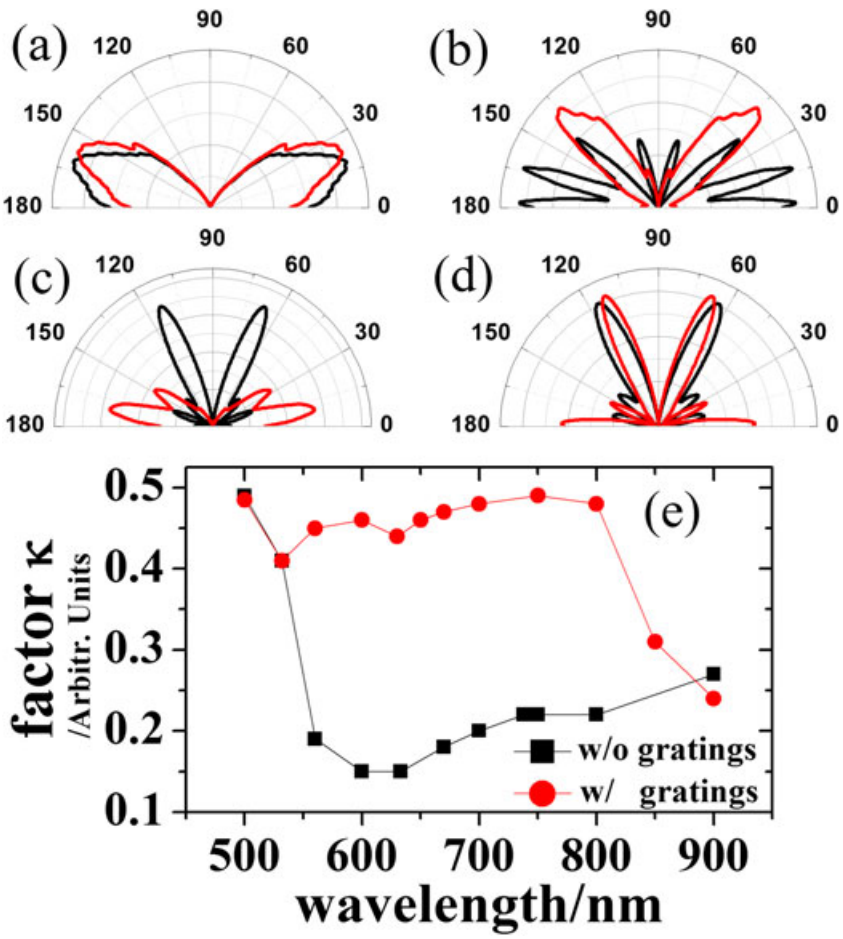

Figure 4. (a–d) Calculated radiation patterns for emission wavelengths at 500 nm, 532 nm, 800 nm, and 900 nm for a tip without (black) and with (red) gratings. (e) Dependence of the factor κ on the dipole emission wavelength. As a result of plasmonic beaming, the corrugated tip exhibits much higher collection efficiency ($\kappa > 0.4$) for a wide range of wavelengths as compared with the bare tip ($\kappa \sim 0.2$).

Journal of RAMAN SPECTROSCOPY

results in the x–z plane. It should be noted that the factor κ defined here is a simple approximation of the collection efficiency for comparison. In practice, this integration should be considered in the full solid angle.[29] For an isolated dipole emitter close to the Au substrate, it exhibits a typical 'doughnut' radiation pattern. Emission spreads over the collection angles with a factor of $\kappa = 0.45$, resulting in great background noise. When we considered a conventional bare tip (total length $L = 2000$ nm) located 10 nm away from the dipole emitter, we found that the main beam angle θ_2 is greater than 60° and that only a small part of the emitted power was collected by the objective ($\kappa = 0.18$),[30,31] which led to a low SNR. When we introduced the concentric metal gratings, we observed an obvious emission beaming effect with the angle θ_m tuned towards 30°; thus, the emitted power can easily be captured by the objective ($\kappa = 0.47$) and resulted in a 2.6-fold increase. This directional emission is due to complex interference of the light emitted directly by the dipole source and surface waves scattered by the surficial corrugated grooves towards the far-field, as previously demonstrated using Green's function.[24]

Figure 4 shows the dependence of the factor κ on the emission wavelength λ. The conventional bare tip has low collection efficiency ($\kappa \sim 0.2$) with varying λ values ranging from 600 to 800 nm. Compared with the bare tip, the emission pattern with the corrugated tip is strongly dependent on the wavelengths (Fig. 4a–d). From $\lambda = 500$ to 800 nm, a dramatically enhanced collection efficiency ($\kappa > 0.4$) can be obtained for a wide range of wavelengths because of the beaming effect from the surface corrugated gratings. At an emission wavelength of 532 nm, the light is directed into a single narrow beam with θ_m at 45° and a full-width at half-maximum (FWHM) of 30° (Fig. 4b). Additional increases in λ to 900 nm produced a rapid decrease in κ to 0.24 and an emission far-field pattern that is quite similar to a conventional bare tip. Furthermore, with a conventional bare tip κ reached up to 0.49 at $\lambda = 500$ nm and exhibited an emission pattern similar to an isolated dipole, which is ascribed to the weak coupling of the antenna–dipole system. This broad band of enhanced directivity makes the antenna design more convenient for nanoscale optical spectroscopy applications, such as molecular fluorescence with large anti-Stokes shifts between the excitation laser and emission wavelength, or a two-photon fluorescence process.

The efficient fluorescence or Raman signal detection is highly desirable and challenging in single molecule detection and analytics.[8] However, the emission patterns discussed previously are omnidirectional in the azimuth angle because of the antenna symmetry, which leads to the loss of more than half of the signal. Pakizeh and Käll[22] postulated that unidirectional emission is possible if an emitter is coupled to the dark mode of two neighboring metallic disks. Considering scanning probe microscopy, we suggested placing two asymmetrical nanorods at the tip end, so that one rod is longer than the other to avoid scanning the surface with two apexes (Fig. 5a). The shorter rod would thus couple more weakly with the emitters. The asymmetric probe can be deconstructed into three main parts: a sharp metal probe with a

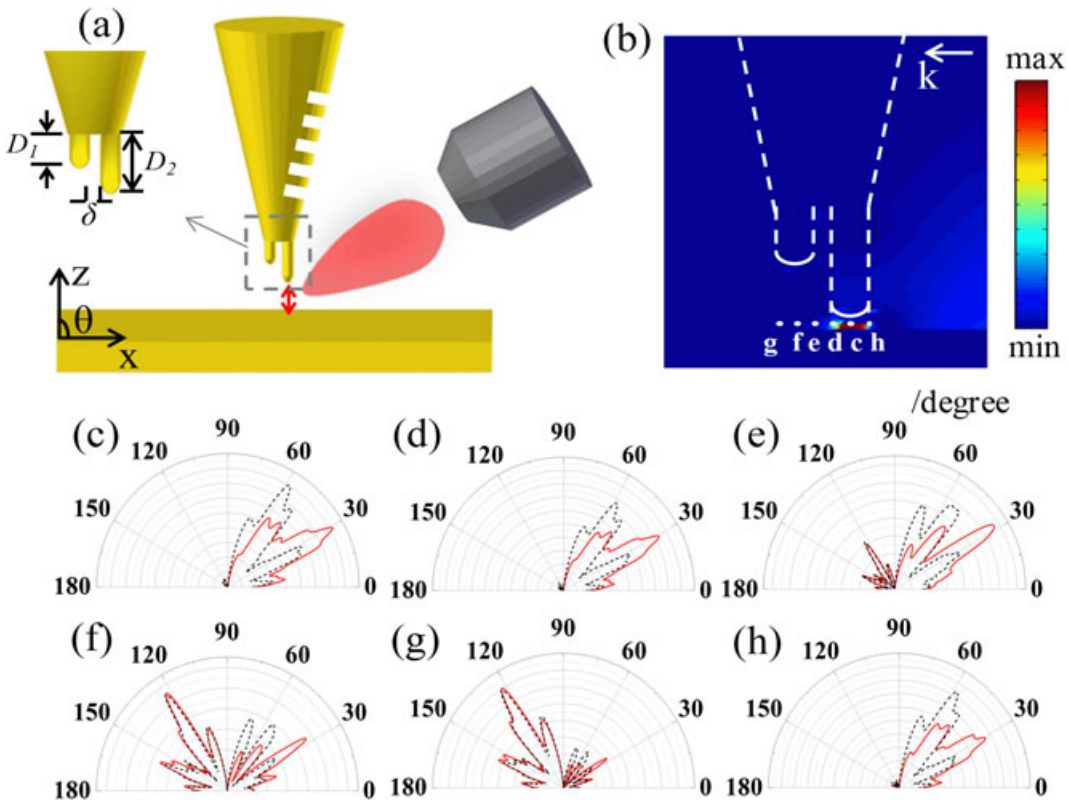

Figure 5. Hybrid asymmetric probe for unidirectional single molecule emission by 2D-FDTD simulations along Cartesian coordinates. (a) Schematics of the hybrid asymmetric probe. (b) Calculated near-field distribution $|E_z|^2/|E_{in}|^2$ in the x–z plane of the asymmetric probe coupled to the Au substrate. In the calculations, a z-polarized plane at 565 nm is incident from $+x$ direction, and the distance between the tip and Au substrate is 4 nm. (c–h) show that the position is dependent on the angular patterns for single emitters placed at (0, −4), (−10, −4), (−20, −4), (−28, −4), (−40, −4), and (10, −4) in nm, respectively, when the tip apex is fixed at (0, 0) nm. The red line indicates the asymmetric tip with gratings and the black dashed line shows results for the bare tip.

tip radius of 25 nm and opening angle of 30°, several grooves milled on one side of the tapered metal tip ($G = g = 390$ nm, $a = 185$ nm, $d = 30$ nm, and $N = 5$), and a dimer resonator (rod radius $r = 10$ nm, length $D_1 = 80$ nm, $D_2 = 40$ nm, and surface–surface distance $\delta = 8$ nm) carved at the tip end. Figure 5b shows the near-field distribution for the asymmetric corrugated tip and demonstrates that the strong electromagnetic field is highly confined in the gap between the tip end and metal surface. The dependence of the angular directivity on the emitter's position is shown in Fig. 5(c)–(d). In Fig. 5c, a *z*-oriented dipole at a wavelength of 800 nm is placed 4 nm away from the longer nanorod. The radiation patterns demonstrated excellent unidirectional emission for both asymmetric tips without and with the surface corrugated gratings. This unidirectional effect results from the near-field coupling of phase shifts between the two rods' dipole mode.[22] While the gratings are responsible for additional beaming light, resulting in a higher collection efficiency ($\kappa = 0.83$) for the corrugated asymmetrical tip. Compared with the conventional TES tip ($\kappa = 0.18$), the factor κ of the asymmetric corrugated tip is almost 5-fold higher. As emitter deviating from the apex (Fig. 5(c)–(g)), the unidirectional effect diminishes and more light is directed towards the left side. Furthermore, the direction of the main radiation lobe is reversed if the emitter is positioned near the shorter nanorod (Fig. 5g). This would suppress the background signal, leading to an increased SNR of the fluorescence or Raman signal, which is helpful for sensitive single molecule detection.

Conclusions

We investigated the emission properties of a 3-dimensional corrugated metal probe with several concentric gratings for a side-illumination TES scheme. The simulation results showed that the angular emission from a *z*-oriented emitter can be directed into a single narrow lobe at a particular polar angle, depending on the antenna parameters and the emission wavelength. This probe also enhanced the localized field intensity approximately 25 times greater than a conventional bare tip. An asymmetric TES tip was also analyzed to further improve the collection efficiency and demonstrated an approximately 5-fold increase above the conventional TES tip from the unidirectional beaming effect. We also explored the dependence of the angular directivity on the emitter's position and found that the emitters away from the apex presented a different emission direction than those directly below the apex. This result implies that a lower nonspecific background is achievable with an asymmetric tip. The highly directional emission of this tip would lead to an increase in the signal-to-noise ratio and less collection time. The proposed probes provide a promising approach for potential applications in optical spectroscopy, analytical chemistry, single molecule sensing, and tip enhanced fluorescence and Raman imaging techniques.

Acknowledgements

This work was supported by the National Key Basic Research Program of China (grant no. 2013CB328703) and the National Natural Science Foundation of China (grant nos. 61422502, 11374026, 91221304, 61521004, 11527901 and 11431017).

References

[1] E. A. Pozzi, M. D. Sonntag, N. Jiang, J. M. Klingsporn, M. C. Hersam, R. P. Van Duyne, *ACS Nano* **2013**, *7*, 885.
[2] E. Bailo, V. Deckert, *Chem. Soc. Rev.* **2008**, *37*, 921.
[3] A. Hartschuh, M. R. Beversluis, A. Bouhelier, L. Novotny, *Phil. Trans. R. Soc. Lond. A* **2004**, *362*, 807.
[4] T. Ichimura, N. Hayazawa, M. Hashimoto, Y. Inouye, S. Kawata, *Phys. Rev. Lett.* **2004**, *92*, 220801.
[5] T. Schmid, L. Opilik, C. Blum, R. Zenobi, *Angew. Chem. Int. Ed.* **2013**, *52*, 5940.
[6] B. Pettinger, P. Schambach, C. J. Villagómez, N. Scott, *Annu. Rev. Phys. Chem.* **2012**, *63*, 379.
[7] A. D. Elfick, A. Downes, R. Mouras, *Anal. Bioanal. Chem.* **2010**, *396*, 45.
[8] R. Zhang, Y. Zhang, Z. C. Dong, S. Jiang, C. Zhang, L. G. Chen, L. Zhang, Y. Liao, J. Aizpurua, Y. Luo, J. L. Yang, J. G. Hou, *Nature* **2013**, *498*, 82.
[9] J. Steidtner, B. Pettinger, *Phys. Rev. Lett.* **2008**, *100*, 236101.
[10] C. Chen, N. Hayazawa, S. Kawata, *Nat. Commun.* **2014**, *5*, 163.
[11] W. Zhang, B. S. Yeo, T. Schmid, R. Zenobi, *J. Phys. Chem. C* **2007**, *111*, 1733.
[12] X. Wang, Z. Liu, M. Zhuang, H. Zhang, X. Wang, Z. Xie, D. Wu, B. Ren, Z. Tian, *Appl. Phys. Lett.* **2007**, *91*, 101105.
[13] J. Stadler, T. Schmid, R. Zenobi, *Nano Lett.* **2010**, *10*, 4514.
[14] N. Mauser, A. Hartschuh, *Chem. Soc. Rev.* **2014**, *43*, 1248.
[15] A. Bek, F. De Angelis, G. Das, E. Di Fabrizio, M. Lazzarino, *Micron* **2011**, *42*, 313.
[16] C. Höppener, Z. J. Lapin, P. Bharadwaj, L. Novotny, *Phys. Rev. Lett.* **2012**, *109*, 17402.
[17] M. Mivelle, T. S. van Zanten, M. F. Garcia-Parajo, *Nano Lett.* **2014**, *14*, 4895.
[18] C. Ropers, C. C. Neacsu, T. Elsaesser, M. Albrecht, M. B. Raschke, C. Lienau, *Nano Lett.* **2007**, *7*, 2784–2788.
[19] Z. Yang, J. Aizpurua, H. Xu, *J. Raman Spectrosc* **2009**, *40*, 1343–1348.
[20] A. Ghimire, E. Shafran, J. M. Gerton, *Sci. Rep.* **2014**, *4*, 6456.
[21] T. H. Taminiau, F. D. Stefani, F. B. Segerink, N. F. Van Hulst, *Nat. Photon.* **2008**, *2*, 234.
[22] T. Pakizeh, M. Käll, *Nano Lett.* **2009**, *9*, 2343.
[23] H. Aouani, O. Mahboub, N. Bonod, E. Devaux, E. Popov, H. Rigneault, T. W. Ebbesen, J. Wenger, *Nano Lett.* **2011**, *11*, 637.
[24] H. Shen, G. Lu, Y. He, Y. Cheng, H. Liu, Q. Gong, *Nanoscale* **2014**, *6*, 7512.
[25] J. Li, J. Mu, B. Wang, W. Ding, J. Liu, H. Guo, W. Li, C. Gu, Z. Li, *Laser Photonics Rev.* **2014**, *8*(4), 602.
[26] A. F. Oskooi, D. Roundy, M. Ibanescu, P. Bermel, J. D. Joannopoulos, S. G. Johnson, *Phys. Commun.* **2010**, *181*, 687.
[27] P. B. Johnson, R. W. Christy, *Phys. Rev. B* **1972**, *6*, 4370.
[28] A. Taflove, S. C. Hagness, *Computational Electrodynamics: The Finite-Difference Time-Domain Method, Third Edition*, Artech House, Norwood, MA, **2005**.
[29] Y. C. Jun, K. C. Y. Huang, M. L. Brongersma, *Nat. Commun.* **2011**, *2*, 283.
[30] T. H. Taminiau, F. D. Stefani, N. F. van Hulst, *Nano Lett.* **2011**, *11*, 1020.
[31] R. Paniagua-Dominguez, G. Grzela, J. G. Rivas, J. A. Sanchez-Gil, *Nanoscale* **2013**, *5*, 10582.